

PAPER

## Magnetic nanocomposites based on phosphorus-containing polymers—structural characterization and thermal analysis

To cite this article: R M Alosmanov *et al* 2018 *Nanotechnology* **29** 135708

View the [article online](#) for updates and enhancements.

### Related content

- [A new perovskite-type NdFeO<sub>3</sub> adsorbent: Synthesis, characterization and As\(V\) adsorption](#)  
Minh Dai Luu, Ngoc Nhiem Dao, Duc Van Nguyen *et al.*
- [One-step continuous synthesis of functionalized magnetite nanoflowers](#)  
G Thomas, F Demoisson, R Chassagnon *et al.*
- [One-step Preparation of graphene oxide/polypyrrole magnetic nanocomposite and its application in the removal of methylene blue dye from aqueous solution](#)  
Ali Afzali Nezhad, Mohammad Alimoradi and Majid Ramezani



## LIVE WEBINAR


NanoRaman: Correlated Tip-Enhanced Optical Spectroscopy and Scanning Probe Microscopy

Thursday 8 March 15.00 GMT

REGISTER NOW!

[physicsworld.com](http://physicsworld.com)

# Magnetic nanocomposites based on phosphorus-containing polymers—structural characterization and thermal analysis

R M Alosmanov<sup>1,2,6</sup>, M Szuwarzyński<sup>2,3</sup>, J Schnelle-Kreis<sup>4</sup>, G Matuschek<sup>4</sup>,  
A M Magerramov<sup>1</sup>, A A Azizov<sup>1</sup>, R Zimmermann<sup>4,5</sup> and S Zapotoczny<sup>2,6</sup> 

<sup>1</sup>Baku State University, Chemistry Department, Z. Khalilov str., 23, Baku, AZ1148 Azerbaijan

<sup>2</sup>Jagiellonian University, Faculty of Chemistry, Gronostajowa 2, 30-387 Krakow, Poland

<sup>3</sup>AGH University of Science and Technology, Academic Centre for Materials and Nanotechnology, al. Mickiewicza 30, 30-059, Krakow, Poland

<sup>4</sup>Joint Mass Spectrometry Centre, Cooperation Group 'Comprehensive Molecular Analytics', Helmholtz Zentrum München, German Research Center for Environmental Health (GmbH), Ingolstädter Landstraße 1, D-85764 Neuherberg, Germany

<sup>5</sup>Joint Mass Spectrometry Centre, Institute of Chemistry, University of Rostock, Rostock, Dr Lorenz Weg 1, D-18051 Rostock, Germany

E-mail: [r\\_alosmanov@rambler.ru](mailto:r_alosmanov@rambler.ru) and [zapotocz@chemia.uj.edu.pl](mailto:zapotocz@chemia.uj.edu.pl)

Received 7 December 2017, revised 23 January 2018

Accepted for publication 29 January 2018

Published 14 February 2018



CrossMark

## Abstract

Fabrication of magnetic nanocomposites containing iron oxide nanoparticles formed *in situ* within a phosphorus-containing polymer matrix as well as its structural characterization and its thermal degradation is reported here. Comparative structural studies of the parent polymer and nanocomposites were performed using FTIR spectroscopy, x-ray diffraction, and atomic force microscopy. The results confirmed the presence of dispersed iron oxide magnetic nanoparticles in the polymer matrix. The formed composite combines the properties of porous polymer carriers and magnetic particles enabling easy separation and reapplication of such polymeric carriers used in, for example, catalysis or environmental remediation. Studies on thermal degradation of the composites revealed that the process proceeds in three stages while a significant influence of the embedded magnetic particles on that process was observed in the first two stages. Magnetic force microscopy studies revealed that nanocomposites and its calcinated form have strong magnetic properties. The obtained results provide a comprehensive characterization of magnetic nanocomposites and the products of their calcination that are important for their possible applications as sorbents (regeneration conditions, processing temperature, disposal, etc).

Keywords: nanocomposites, magnetic nanoparticles, magnetic force microscopy, thermal analysis

(Some figures may appear in colour only in the online journal)

## 1. Introduction

The unique physical and chemical properties of nanoparticles (NPs) that are related to quantum size effects and large surface

area/energy are the major factors influencing a growing interest in fundamental studies and applications of NPs [1–3]. While NPs have a strong tendency to agglomerate [4, 5] there have been a number of methods developed for their stabilization by using various materials, including inorganic compounds [6], surfactants [7], and polymers [8, 9]. The incorporation of NPs in

<sup>6</sup> Authors to whom any correspondence should be addressed.

polymer or other matrices allow obtaining new nanocomposite materials [6–9]. Among the broad spectrum of such systems magnetic nanocomposites (MNCs) have gained significant attention due to their intrinsic magnetic properties [10–12]. Magnetic NPs due to their small size commonly exhibit superparamagnetic properties that make them useful as e.g. contrast agents in magnetic resonance imaging (MRI) [13, 14], drug carriers [15, 16], or in hyperthermia treatment [17]. MNCs combining magnetic properties of NPs and tunable porous structure and mechanical properties of the polymer matrix have been considered as desirable materials for various application in e.g. information technology, telecommunications [18, 19], catalysis [20], MRI [13, 21], biomedicine, and environmental remediation [22–24]. Taking advantage of soft polymer matrices nanocomposites with well-dispersed magnetic NPs may be formed overcoming common difficulties related to their aggregation that often leads to diminishing their magnetic properties [25]. Therefore, the design and preparation of various magnetic nanostructures have been the subject of numerous studies [26, 27].

MNCs can be generally prepared by either embedding the preformed magnetic NPs in a soft polymer matrix or by their synthesis *in situ* within the porous polymer material using appropriate soluble precursors. Due to diffusion limits, synthesis of magnetic NPs from their soluble precursors in a polymer matrix seems to be favorable for reaching uniform distribution of NPs in MNCs. Such composites may be obtained through the hydrolysis or reduction of metal salts in the presence of polymers [28, 29]. Ziolo *et al* developed a method to synthesize  $\gamma$ -Fe<sub>2</sub>O<sub>3</sub> NPs in a commercial ion exchange resin [30]. For this purpose ion exchange of iron ions by cross-linked sulfonated porous polystyrene was carried out followed by precipitation of iron oxide NPs in a polymer matrix. This method was then applied to obtain MNCs based on cross-linked polymers such as anions and cations exchangers [31–35] as well as macromolecular oxidizers [36] that have numerous environmental applications. For example, the sorption properties of the synthesized MPCs for the oxyanions of arsenic [31], Cu<sup>2+</sup>, Zn<sup>2+</sup> [32], and sulfide [33] have been investigated.

Thermal analytical methods are widely used in the study of the relationship between the composition and processing temperature of materials as well as their thermal degradation (TD). This is particularly important for materials used as sorbents. First of all, many processes involving such materials are carried out at relatively high temperatures and may be accompanied by some structural changes of the sorbents. Moreover, characterization of the sorbent materials using thermal methods is important for their regeneration or calcination (e.g. prior to disposal). Finally, if the sorption materials are polymeric composites, their thermal analysis allow identifying the impact of various components on the thermal stability of the polymer.

This paper presents the synthesis and TD of new MNCs based on phosphorus-containing polymer (PhCP). PhCP was applied as an efficient sorbent of heavy metal ions [37] and the formation of MNCs may be the way of their efficient separation from the environment without the necessity of filtration [38]. PhCP was synthesized by chemical

modification (oxidative chlorophosphorylation reaction) of an industrial polymer—butadiene rubber (BR). In this work structural characterization and TD of the PhCP and respective MNCs based on PhCP were investigated. A kinetic analysis of the TD process by means of the Friedman and Ozawa–Flynn–Wall (OFW) kinetic methods is also presented.

## 2. Experimental

### 2.1. Materials

The BR was purchased from the Voronezh Synthetic Rubber Manufactory (Russia). PCl<sub>3</sub>, CCl<sub>4</sub>, p-xylene, FeCl<sub>2</sub> · 4H<sub>2</sub>O, FeCl<sub>3</sub> · 6H<sub>2</sub>O, NaOH (all p.a.) were supplied by Gorex Analyt GmbH and used without further purification. Oxygen was purified (removal of traces of water) by passing it through concentrated sulfuric acid (VI) (Gorex Analyt GmbH). All aqueous solutions used for the experiments were prepared using distilled water.

### 2.2. Synthesis of the PhCP

The synthesis of the PhCP was realized following our previously reported method [39]. Namely, a 5% solution of BR in CCl<sub>4</sub> was mixed with PCl<sub>3</sub> (BR:PCl<sub>3</sub>, 1:5 w/w ratio). The reaction was carried out at room temperature for 8 h under oxygen flow (7 L · h<sup>-1</sup>) and after its completion p-xylene was added to the reaction solution. Then, the liquid components (CCl<sub>4</sub>, POCl<sub>3</sub>, unreacted PCl<sub>3</sub>) were evaporated under intensive stirring using a vacuum pump leaving solid phosphochlorinated BR in the form of swollen powder (PChBR). This product was a cross-linked functional polymer (–P(O)Cl<sub>2</sub>, phosphonyldichloride and –OP(O)Cl<sub>2</sub>, phosphoryldichloride groups) with P–Cl bonds. Then the mixture of PChBR and p-xylene was added to ice water for the separation of the cross-linked polymer. The separated polymer was subjected to hydrolysis that was carried out at 50 °C for 4 h with continuous stirring. The product was filtered and washed with distilled water several times until a neutral pH was reached. Then it was washed with acetone and dried in air and then placed under a vacuum at 40 °C. The final product (PhCP) was obtained in a form of a dark-brown powder.

### 2.3. Synthesis of the MNC (Ph-MNC) based on PhCP

A previously reported synthetic procedure has been modified here [38]. Namely, ferric and ferrous chlorides (with a molar ratio 2:1) were dissolved in water with a total concentration of 0.1 M of iron ions. Then, the 100 ml mixture of solutions of iron salts was added to the 1.0 g of PhCP. The suspension was stirred for 2 h and then the polymer was filtered off, washed thoroughly with distilled water, and dried in air. The 2 M solution of sodium hydroxide (100 ml) was added to the air-dried PhCP with Fe<sup>2+</sup> and Fe<sup>3+</sup> ions. The reaction was carried on for 1 h at 80 °C under argon atmosphere with constant and vigorous stirring. The obtained pure black Ph-MNC nanocomposite was separated using an external magnetic field (neodymium magnet) and was treated with 1 M of HCl

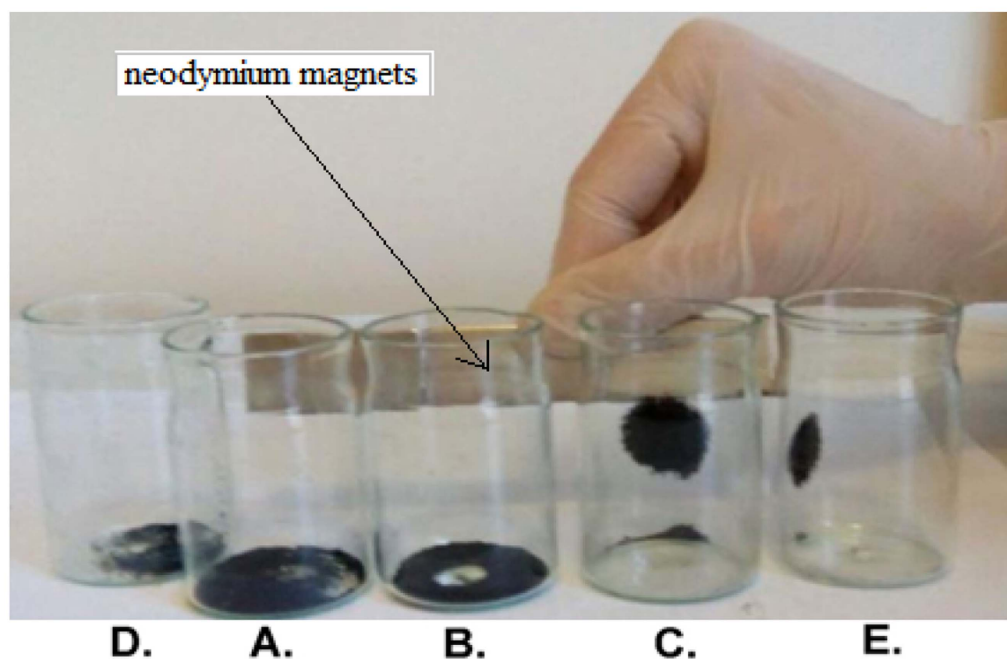
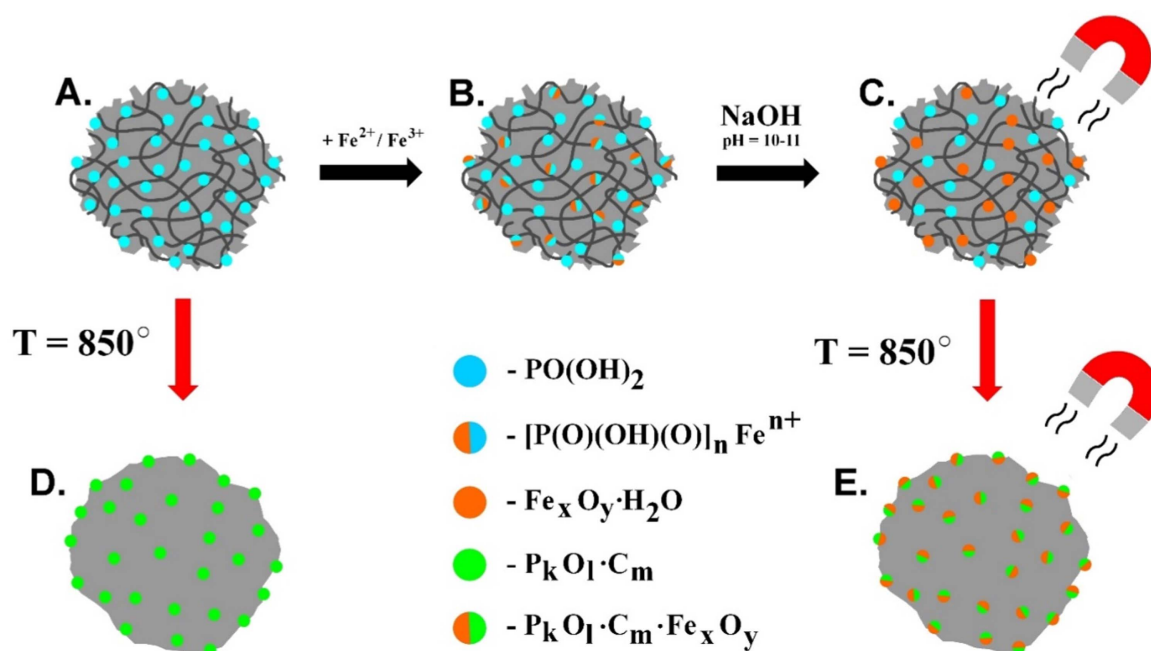


**Figure 1.** Schematic presentation of the preparation of the Ph-MNC from PhCP, their calcination as well as a photograph illustrating the powder forms and magnetic properties of the respective materials: (a) PhCP, (b) PhCP with adsorbed iron ions, (c) Ph-MNC, (d) calcinated PhCP (C-PhCP), and (e) calcinated Ph-MNC (C-Ph-MNC).

solution for the removal of the surface attached particles. Afterwards, the Ph-MNC was washed several times with water and ethanol, separated via centrifugation, and finally dried in a vacuum oven at  $50^\circ\text{C}$ . The PhCP and Ph-MNC were scuffed in an agate vessel up to a disperse state (35–50 mesh).

#### 2.4. Characterization methods

For determination of the content of iron in the Ph-MNC, the sample was treated with a mixture of concentrated HCl and

$\text{HNO}_3$  (1:1) followed by appropriate dilution of the formed solution and analyzed using an atomic-emission spectrometer (Optima 2100 DV, Perkin-Elmer). X-ray diffraction (XRD) patterns of the Ph-MNC were recorded on an automatic diffractometer 'D2 PHASER' (Bruker) at room temperature ( $\text{Cu-K}\alpha 1$ ,  $\lambda = 1.54060 \text{ \AA}$ ). FTIR spectroscopy measurements were performed using a Thermo Nicolet iS10 FTIR spectrometer (Thermo Scientific) with ATR equipment (SMART iTX). The samples were vacuum dried before the measurements. Spectra were baseline corrected and normalized using Omnic v9.0 software (Thermo Scientific). Atomic



**Figure 2.** Photograph showing the recovery of MNC from its suspension by application of external magnetic field (neodymium magnets).

force microscopy (AFM) images were obtained with the Dimension Icon microscope (Bruker) working in air using a tapping mode. Magnetic force microscopy (MFM) images were acquired using the same microscope working in the lift mode. In all measurements magnetic Co/Cr coated standard silicon cantilevers with nominal spring constant of  $2 \text{ N m}^{-1}$  were used. Before scanning the cantilevers were magnetized with a small magnet. All MFM images were taken within the lift (surface–tip) distance of 100 nm.

Thermogravimetric analyses (TGA) were performed on a NETZSCH TG 209/cell Thermal Analysis System between  $20 \text{ }^\circ\text{C}$  and  $850 \text{ }^\circ\text{C}$  with the use of  $\text{Al}_2\text{O}_3$  crucibles. The measurements were carried out under the flow of synthetic air ( $35 \text{ ml min}^{-1}$ ) at five different heating rates ( $\beta = 1, 5, 10, 15,$  and  $20 \text{ K min}^{-1}$ ) for the granulated samples. The samples after the measurements (heated up to  $850 \text{ }^\circ\text{C}$ ) were further investigated (calcinated samples).

### 3. Results and discussion

In our previous study PhCP materials were described in detail [39]. According to the results of solid state  $^1\text{H}$ ,  $^{13}\text{C}$ , and  $^{31}\text{P}$  NMR analysis it was established that PhCP contains phosphonate ( $-\text{P}(\text{O})(\text{OH})_2$ ) and phosphate ( $-\text{OP}(\text{O})(\text{OH})_2$ ) groups. Chlorine and hydroxyl groups directly connected to the carbon atoms of the main macromolecular chain:  $-\text{CHCl}$ ;  $-\text{CH}(\text{OH})$  are also present there. The presence of functional groups in the cross-linked PhCP as well as its porous structure enables adsorption of iron ions and the subsequent formation of magnetic particles in the polymer matrix leading to Ph-MNC (figures 1(a)–(c)). Such nanocomposites, thanks to the presence of magnetic particles, can be easily isolated from the suspension just by applying a magnetic field (see figure 2). Such capability is very important for possible applications of PhPC-based materials in e.g. catalysis or environmental

remediation. The structural and magnetic properties of the obtained Ph-MNC were investigated using the FTIR and AFM-MFM techniques. Moreover, to study the distribution of the magnetic particles XRD analysis was performed. Additionally, parent PhCP material and the obtained Ph-MNC nanocomposites were thermally treated (up to  $850 \text{ }^\circ\text{C}$ ) using TGA (figures 1(a)–(d) and (c)–(e)). As shown in the photograph in figure 1 only the nanocomposite Ph-MNC (flask C) and its calcinated form, C-Ph-MNC, (flask E) exhibit magnetic properties. FTIR and AFM-MFM measurements were performed for the C-PhCP and the C-Ph-MNC as well.

#### 3.1. XRD studies

The Ph-MNC was found to have a generally amorphous structure as was shown using XRD (see figure 3). The diffractogram of the Ph-MNC exhibits several broad peaks at  $2\theta$  equal to ca.  $19^\circ, 20.5^\circ, 33^\circ, 36^\circ, 37^\circ, 40^\circ, 51^\circ, 54^\circ$  and  $59.5^\circ$  that could be assigned to crystallographic planes of various forms of iron oxides such as magnetite ( $\text{Fe}_3\text{O}_4$ ), maghemite ( $\gamma\text{-Fe}_2\text{O}_3$ ), hematite ( $\alpha\text{-Fe}_2\text{O}_3$ ), goethite ( $\text{FeO}(\text{OH})$ ), and ferrihydrite [40–42]. While the synthetic methods employing both  $\text{Fe}^{3+}$  and  $\text{Fe}^{2+}$  ions should lead to the formation of magnetite the presence of other forms of iron oxide cannot be excluded as e.g. magnetite and maghemite form a crystallographically isomorphous spinel structure. Moreover, magnetite very slowly oxidizes to maghemite at room temperature [43]. XRD-based identification of a particular iron oxide in nanosized particles is difficult because of significant peak broadening due to the size effect. It is also known that the hydrolysis of acidic solutions of iron salts can result in various iron oxides and oxohydroxides, depending on the reaction conditions. The fast hydrolysis of  $\text{Fe}^{3+}$  solution typically leads to amorphous non-stoichiometric hydrated oxohydroxide  $\text{Fe}_2\text{O}_3 \cdot n\text{H}_2\text{O}$ , which is also known as ferrihydrite [44]. Nevertheless, the presence of various types of iron oxides does not reduce the value of the resulting composite as almost all of them may also serve as absorbents [45].

#### 3.2. Comparative structural characteristics of PhCP and Ph-MNC

**3.2.1. FTIR analysis of PhCP and Ph-MNC.** The FTIR spectra of the PhCP and Ph-MNC are shown in figure 4. In the spectrum of the PhCP the IR bands in the  $1200\text{--}1150 \text{ cm}^{-1}$  region can be assigned to  $-\text{P}=\text{O}$  groups vibrations. The IR bands at  $1702, 2864,$  and  $3394 \text{ cm}^{-1}$  are attributed to OH vibration in the  $-\text{PO}(\text{OH})_2$  groups. The IR band at  $986 \text{ cm}^{-1}$ , corresponding to the C–O–P bond, indicates the attachment of the  $-\text{PO}(\text{OH})_2$  group to the polymer chain via oxygen [38].

Comparison of the of PhCP and Ph-MNC spectra indicates significant differences in the regions of  $400\text{--}1100$  and  $3000\text{--}3600 \text{ cm}^{-1}$ , while characteristic absorption bands of the Fe–O bond of iron oxides (mainly in magnetite and maghemite) are reported to be located between  $400$  and  $700 \text{ cm}^{-1}$  [46, 47]. The band of the Fe–O bond in the bulk iron oxides that is located at  $570 \text{ cm}^{-1}$  [48] was shifted in the

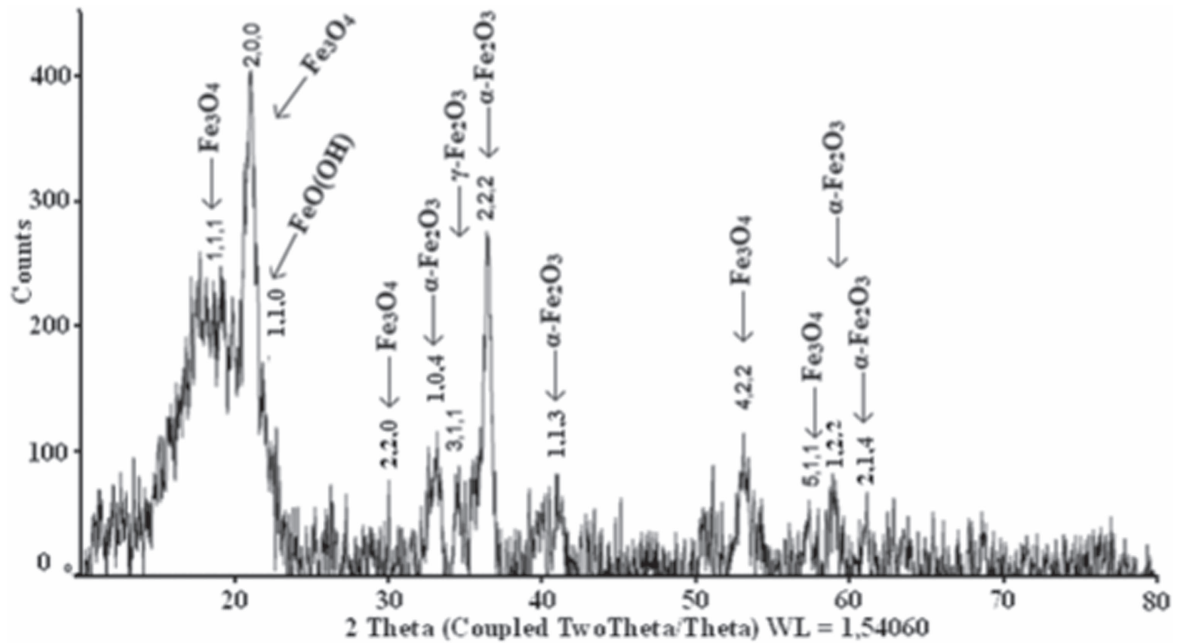


Figure 3. XRD patterns of the Ph-MNC nanocomposite.

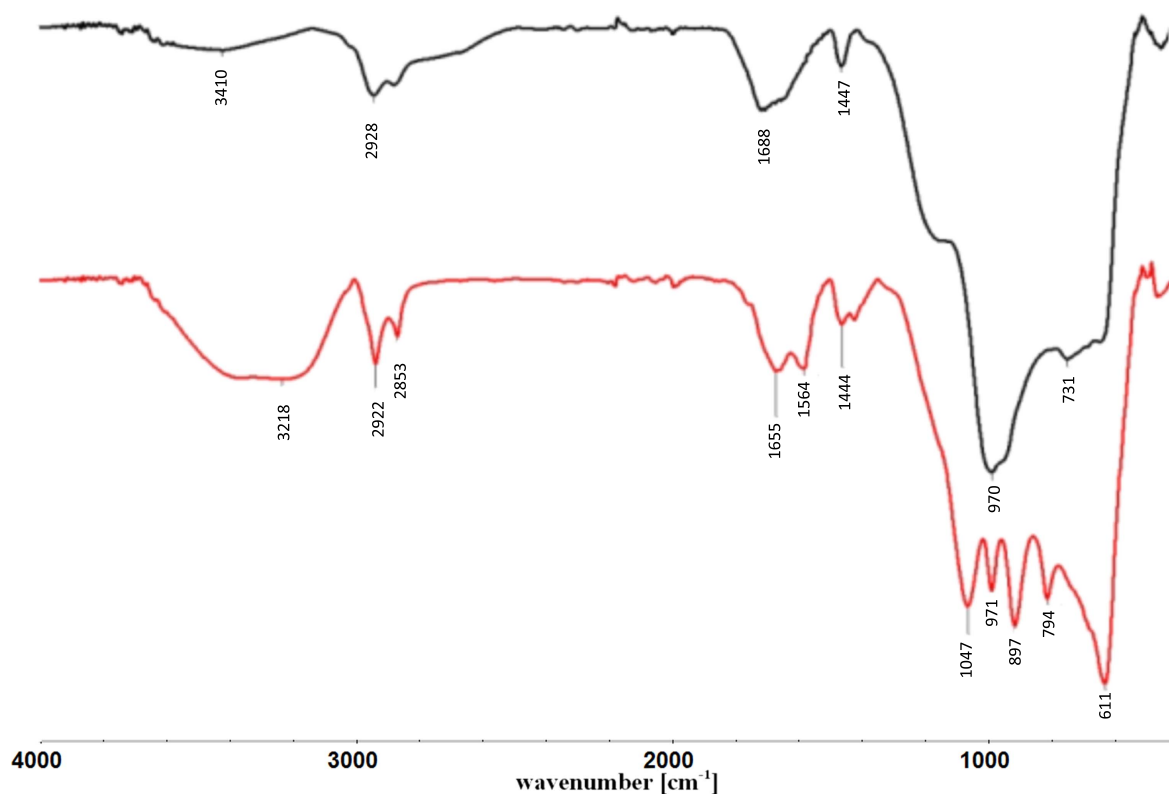


Figure 4. FTIR transmission spectra of the PhCP (black) and Ph-MNC (red).

nanocomposite system to higher wavenumbers ( $611\text{ cm}^{-1}$ ) that is common for iron oxide NPs [49]. Besides this, the data also reveal the presence of a characteristic IR band at  $\sim 1047\text{ cm}^{-1}$ , corresponding to inner-sphere Fe–O–P bonds [50]. This band indicates that the iron oxide particle in Ph-MNC may covalently bond via surface hydroxyl groups to polymeric phosphorous containing groups. The sharp bands

located at  $794$  and  $897\text{ cm}^{-1}$  can be assigned to the vibrations of the free –OH groups on the surface of the iron oxide particles. Moreover, differences between the spectra of the PhCP and Ph-MNC in the region of  $3000\text{--}3600\text{ cm}^{-1}$  can be explained by the same reason. The broad band in the region of  $3300\text{--}3600\text{ cm}^{-1}$  can be also be attributed to water adsorbed on the iron oxide particles [51].

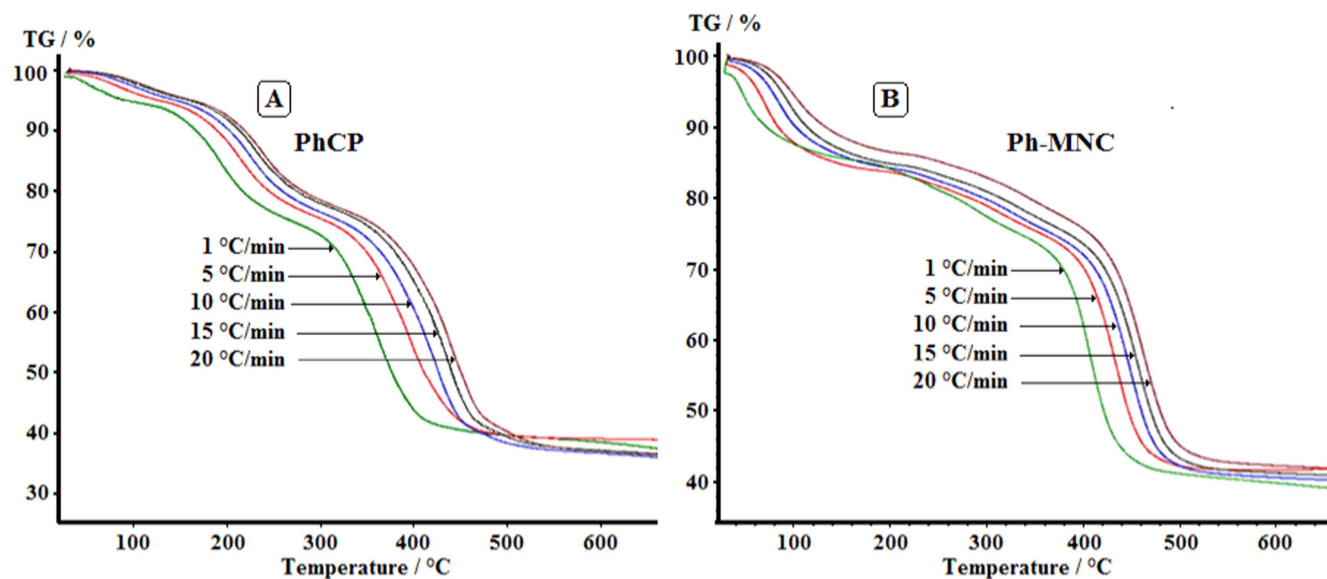


Figure 5. TG curves of the PhCP (a) and Ph-MNC (b) with different heating rates.

Table 1. Mass change and characteristic temperatures of TD for PhCP and Ph-MNC at different heating rates.

Samples	Heat rate, K	Mass, mg	First step				Second step				Third step				Residue at 850 °C %
			$T_i$	$T_m$	$T_f$	$\Delta m, \%$	$T_i$	$T_m$	$T_f$	$\Delta m, \%$	$T_i$	$T_m$	$T_f$	$\Delta m, \%$	
			PhCP	1	10.365	36	44	105	4.2	105	194	274	19.8	274	
	5	10.332	36	83	129	4.4	129	214	294	19.1	294	353	560	36.8	36.3
	10	10.356	36	102	140	4.5	140	226	306	19.1	306	424	580	39.3	31.5
	15	10.428	36	108	149	4.4	149	232	313	18.3	313	436	590	40.0	33.0
	20	10.050	36	113	156	4.6	156	238	319	18.0	319	442	600	40.4	32.8
Ph-MNC	1	10.337	36	45	160	11.7	160	290	325	9.8	325	407	500	34.4	35.2
	5	10.340	36	70	186	14.6	186	313	345	8.1	345	434	560	34.0	43.0
	10	10.246	36	84	201	15.0	201	329	358	8.5	358	448	580	34.9	39.0
	15	9.887	36	93	206	14.8	206	338	368	8.6	368	456	590	34.8	39.9
	20	10.089	36	101	210	13.4	210	346	372	8.4	372	463	600	35.6	40.8

$T_i$ —initial degradation temperature, °C.

$T_m$ —temperature corresponding to the maximum rate of degradation, °C.

$T_f$ —final degradation temperature, °C.

3.2.2. Identification of the thermal decompositions steps of PhCP and Ph-MNC. Thermogravimetric (TG) curves for the PhCP and Ph-MNC samples are shown in figure 5. The degradation stages and the weight losses, at various heating rates, derived from the TG curves are listed in table 1.

The degradation of the samples proceeds in general three stages. Visual inspection of the plots of samples and values of weight loss shows that the degradation of the PhCP and the Ph-MNC proceed differently. This difference is clearly visible in the first two stages of degradation. The temperature range in the first stage is between ca. 30 and 160 °C and the average weight loss is equal to 4.3 wt.% for the PhCP. Based on the experimental condition (synthesis, pre-treatment procedure) and structure of the samples (porous and cross-linked), weight loss at this stage is due to elimination of physically adsorbed water existing in the pores and of the hydrogen-bonded water with the functional groups. The first stage of the Ph-MNC was

recorded in a wider temperature range (30 °C–210 °C) in comparison to the PhCP. The values of weight loss for the composite were more than three times larger (table 1, 11 ÷ 15 w/w.%). This fact may be explained by the presence of magnetic NPs in the pores and on the surface of the PhCP. Magnetic NPs possess hydroxyl groups in their structure that may bound additional water molecules.

The final degradation temperature of the second stage is in the ranges of 274 °C–319 °C, and 325 °C–372 °C for the PhCP and the Ph-MNC, respectively. This stage is characterized by a large change in the TG curve slopes for the PhCP, while for the Ph-MNC this segment is different. Those results were also confirmed by a roughly twice larger weight loss for the PhCP (18 ÷ 20 w/w.%) than the one observed for the Ph-MNC (8 ÷ 10 w/w.%). This step of thermal degradation may be assigned to the dehydration processes, the anhydridization of phosphonate and phosphate groups, and the elimination of

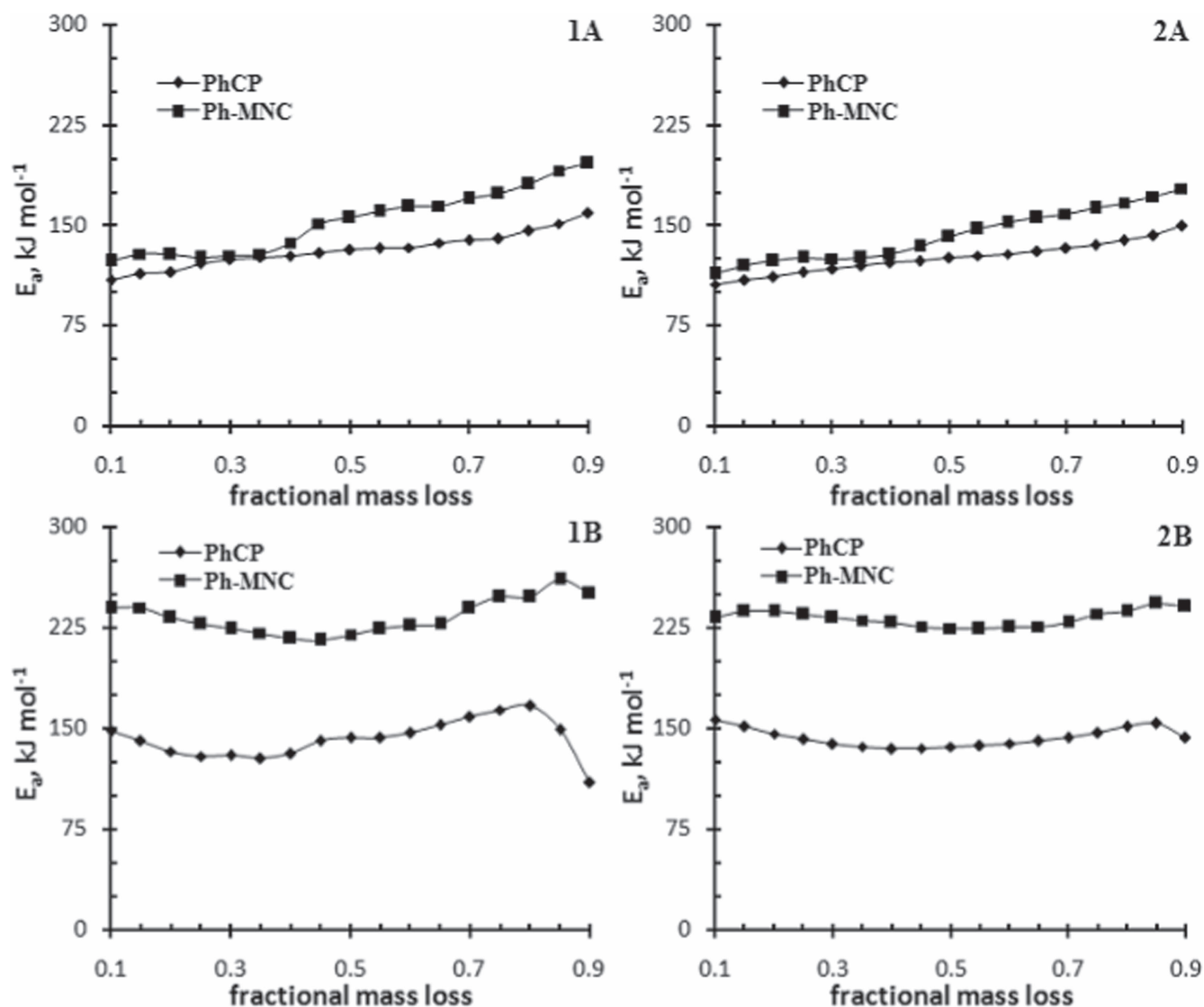


**Figure 6.** Variation of  $E_a$  versus fractional mass loss ( $\alpha$ ) for the second (a) and third (b) degradation stages of samples based on the Friedman (1) and OFW (2) methods.

**Table 2.** The kinetics parameters obtained by the Friedman and OFW methods for the PhCP and the Ph-MNC.

Sample	Step I				Step II				Step III			
	$E_a$ , kJ · mol <sup>-1</sup>		$A$ , s <sup>-1</sup>		$E_a$ , kJ · mol <sup>-1</sup>		$A$ , s <sup>-1</sup>		$E_a$ , kJ · mol <sup>-1</sup>		$A$ , s <sup>-1</sup>	
	Friedman	OFW	Friedman	OFW	Friedman	OFW	Friedman	OFW	Friedman	OFW	Friedman	OFW
PhCP	62	64	$2.9 \cdot 10^7$	$2.8 \cdot 10^7$	131	125	$1.5 \cdot 10^{11}$	$7.7 \cdot 10^{10}$	142	143	$2.0 \cdot 10^8$	$3.6 \cdot 10^8$
Ph-MNC	66	69	$3.4 \cdot 10^7$	$3.4 \cdot 10^7$	153	143	$2.7 \cdot 10^{11}$	$6.5 \cdot 10^{10}$	233	232	$3.9 \cdot 10^{14}$	$4.9 \cdot 10^{14}$

hydrogen chloride. The products of the degradation process may interact with magnetite particles, so the weight loss of the composite is less than that of the sole polymer.

At higher temperatures the third weight loss stage for both samples is characterized by a sharp change in the TG curve slopes, especially in the case of Ph-MNC. The weight loss increases similarly for both materials reaching the average level of  $37.0 \pm 3.0\%$ . This stage could be attributed to the elimination of side groups from the polymer chains,

random depolymerization, and detachment of larger organic molecules that could be formed in the second stage. At such high temperatures cracking and gasification processes occur as well. The obtained results show that magnetic NPs do not significantly affect the values of weight loss at the third degradation stage indicating that the particles do not react with the degradation products or newly formed intermediate compounds decompose again. Finally, the residual amounts of the samples were compared. The mass of residue for the



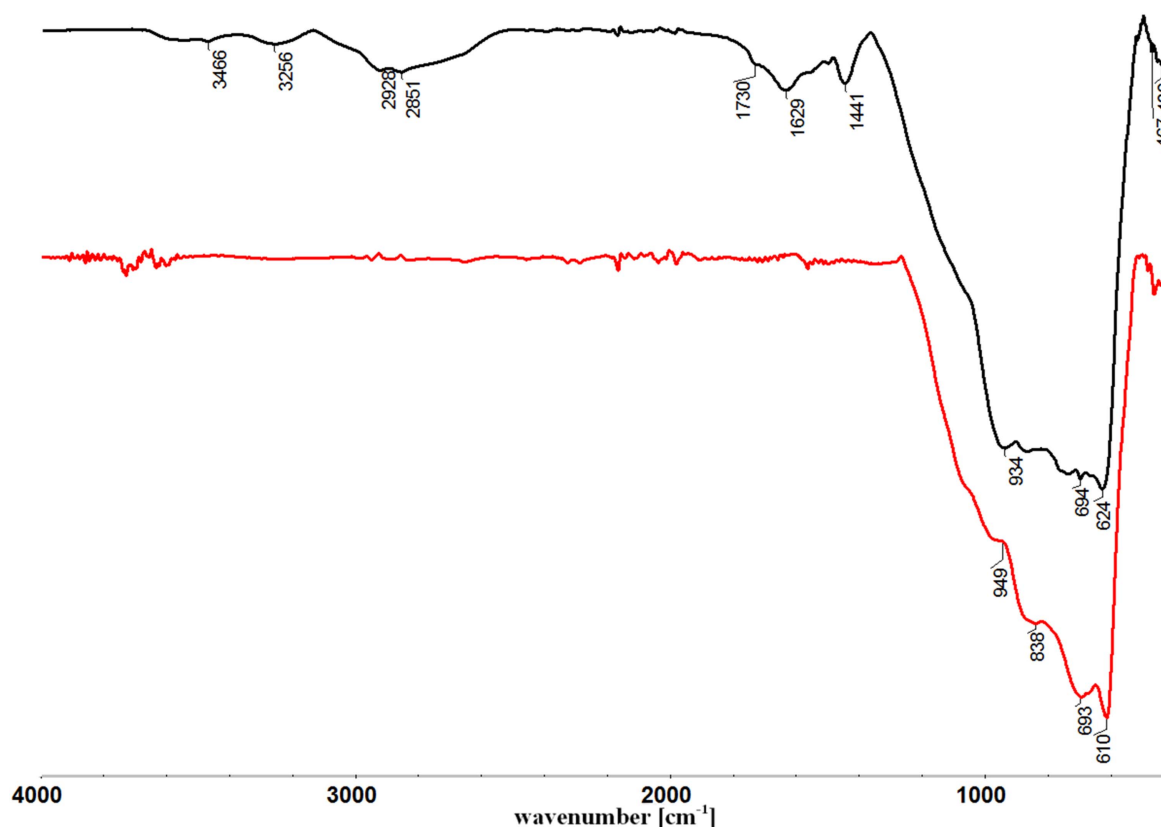


Figure 7. FTIR spectra of the C-PhCP (black) and the C-Ph-MNC (red).

Ph-MNC was ca. 7%–9% (with respect to the starting masses) higher than for the PhCP that is in good agreement with the amount of iron in the composite determined before TD (6%).

### 3.3. Kinetics of the TD of PhCP and Ph-MNC

According to the non-isothermal kinetic theory, TD of polymers can be expressed by the following equation (1):

$$\frac{d\alpha}{dT} = \frac{1}{\beta} A e^{-\frac{E_a}{RT}} f(\alpha) \quad (1)$$

where  $f(\alpha)$  is the differential expression of a kinetic model function,  $\alpha$  is the fractional mass loss,  $\beta$  is the heating rate, and  $E_a$  and  $A$  are the so-called activation energies and pre-exponential factor for the decomposition reaction, respectively,  $R$  is the general gas constant. The fractional mass loss is a measure of reaction progress as a function of time or temperature. For non-isothermal TGA, the fractional mass loss can be calculated with the formula (2):

$$\alpha = \frac{m_0 - m_T}{m_0 - m_\infty}, \quad (2)$$

where  $m_0$  is the initial sample weight,  $m_T$  is the sample weight at temperature  $T$ , and  $m_\infty$  is the final sample weight.

In the study of the evaluation of the kinetic parameters ( $E_a$ ,  $A$ ) the OFW [52–54] and Friedman [55] methods were chosen. These methods can be successfully used to study TD kinetics for polymers, blends, and composites, without any *a priori* knowledge of the reaction mechanism. The kinetic

parameters were calculated using the Netzsch Thermokinetics Software [56]. The mean values of  $E_a$  and  $A$  for the studied samples are presented in table 2.

The values of the kinetic parameters calculated by the two methods (see table 2) for the first degradation stage are very similar for both materials. The overall  $E_a$  of the first degradation stage was found to be in the range of 60–70 kJ mol<sup>-1</sup>. The values of the kinetic parameters of the second TD stage are higher than for the previous stage. The  $E_a$  of the PhCP was 131, 125 kJ mol<sup>-1</sup> and that of Ph-MNC was equal to 153, 143 kJ mol<sup>-1</sup>, based on the Friedman and OFW methods, respectively. This indicates that the presence of magnetic NPs in the composite influences  $E_a$  likely due to larger problems with the removal of the decomposition products from the reaction medium. This effect becomes more pronounced in the third stage of the degradation process. The  $E_a$  for the composite is almost 100 kJ mol<sup>-1</sup> higher than for the PhCP.

Thus, during the TD process a significant change associated with the structure of the samples takes place in the second and third stages. Therefore, to have a more complete image of the thermal behavior of the studied samples, the variation of  $E_a$  versus  $\alpha$  during the second and third degradation stages was plotted in figure 6. The comparison of the  $E_a$  versus  $\alpha$  plot in figure 6 leads to the conclusion that the second stage is the crucial degradation process for the samples because it is non-stationary in non-isothermal conditions. By increasing the temperature a continuous increase of  $E_a$

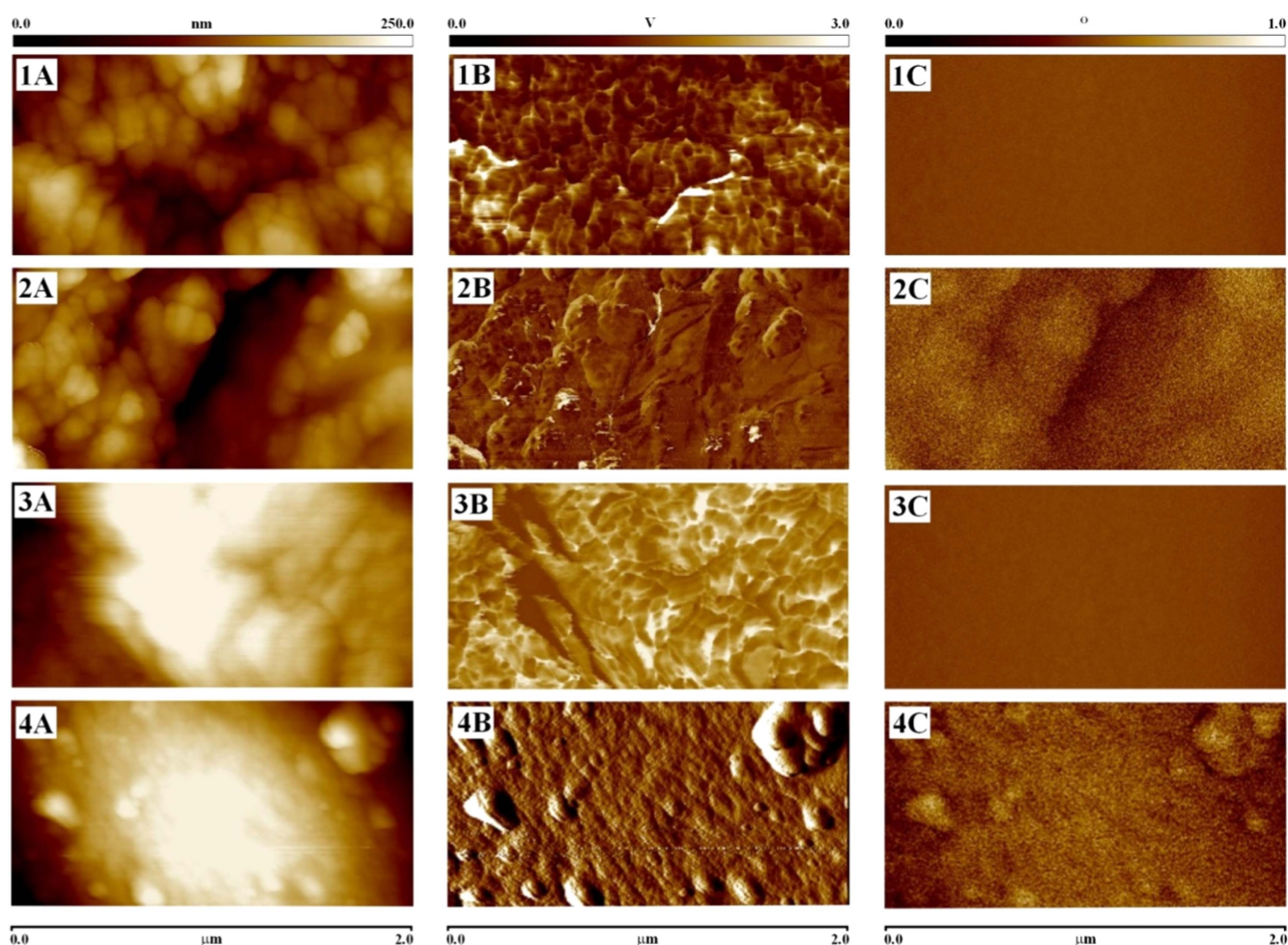


**Figure 8.** AFM images of the topography (a), mechanical phase (b), and MFM (magnetic) phase (c) for 1.—PhCP, 2.—Ph-MNC, 3.—C-PhCP, and 4.—C-Ph-MNC.

was observed in the second stage. The results also show that the  $E_a$ - $\alpha$  plot for the composite differs from the corresponding plot of the PhCP (compare the slopes). Thus, magnetic NPs seem to change the mechanism of the polymer degradation.

The variations of  $E_a$  taking place in the third degradation stage are plotted in figure 6(b). The  $E_a$  values for both samples exhibit sinusoidal variation with  $\alpha$  indicating changes in the degradation pathway. In this degradation stage, the decrease of  $E_a$  (in the range  $0.35 < \alpha < 0.8$ ) could be also caused by the loss of the degradation products formed by the rupture of the functional groups attached to the polymer backbone. This variation of  $E_a$ , characterized by a dramatic increase or decrease as a function of  $\alpha$  could be assigned either to some competitive processes or to the depolymerization in non-stationary conditions.

Finally, in the comparison of the  $E_a$ - $\alpha$  plots obtained by the two applied methods very similar behavior was observed in the second and third stages. Thus, it would appear that either the differential (Friedman) or integral (OFW) method can provide a satisfactory mathematical approach to establish the kinetic parameters for the TD of functional polymer as well as the studied composite.

### 3.4. FTIR analyses of the calcinated polymer and nanocomposite

To make clear how the presence of magnetic NPs influence the TD process the calcinated polymer (C-PhCP) and composite (C-Ph-MNC) were investigated and compared. In the spectrum of the C-PhCP (see figure 7) the peaks corresponding to the  $-\text{CH}_2-$  ( $2928\text{ cm}^{-1}$ ),  $-\text{CH}-$  ( $2851\text{ cm}^{-1}$ ), and  $\text{C}-\text{O}-\text{C}$  ( $1090\text{ cm}^{-1}$ ) groups as well as the bands attributed to phosphorus oxide in the range of  $700\text{--}1000\text{ cm}^{-1}$  [57] were observed. In the spectrum of the C-Ph-MNC, with the exception of the peaks corresponding to phosphorus oxide and iron oxide, the other bands vanished. This result can be explained by the catalytic effect of the iron oxide. According to the literature nanosized transition metallic oxides such as iron oxide, magnetite, hematite, and maghemite are materials that may play a role in the catalysts in TD reactions [58].

### 3.5. AFM-MFM characterization of the PhCP and the Ph-MNC and their calcinated forms

MFM was used to confirm the magnetic properties of the obtained structures and determine the size of the magnetic particles (see figure 8). The microscope worked in the

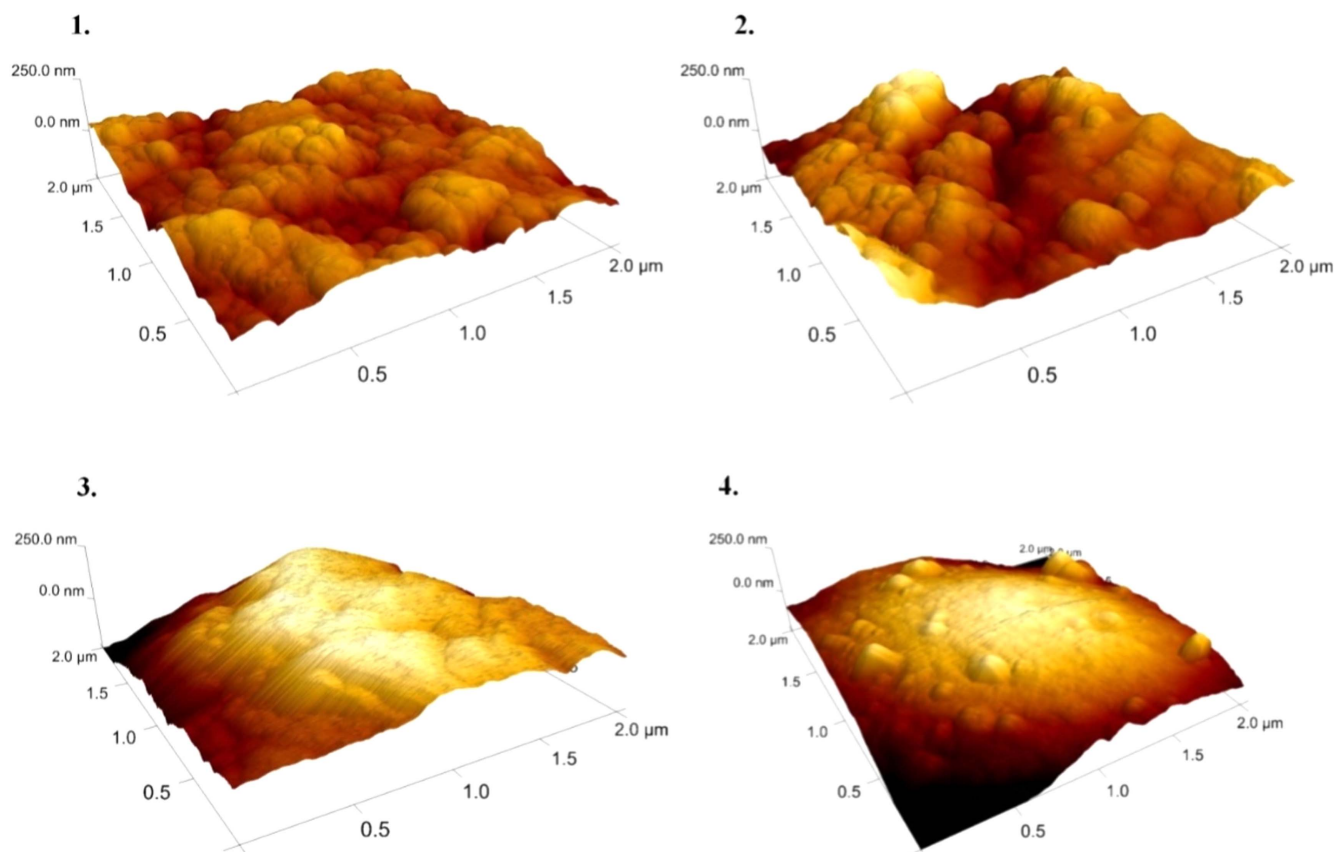


**Figure 9.** 3D AFM topography images of 1.—PhCP, 2.—Ph-MNC, 3.—C-PhCP, and 4.—C-Ph-MNC.

interleave mode which allowed obtaining AFM topography and phase images as well as MFM magnetic phase image form exactly the same areas on the sample. Only the samples with incorporated magnetic particles (Ph-MNC, C-Ph-MNC) revealed signal in the MFM phase images. It can only be observed for the samples possessing magnetic domains which are able to interact with the magnetized tip. This clearly indicates that the investigated nanocomposite samples exhibit strong magnetic properties and that the distribution of the particles is relatively uniform. Samples without magnetic NPs (PhCP, C-PhCP) even they are characterized by nanostructured surface (see figures 8(1a) and (3a)) do not exhibit any magnetic properties (see figures 8(1c) and (3c)).

Differences in topography between initial samples (before calcination) and its calcinated forms were studied using AFM. The biggest differences were observed for the same types of materials before and after thermal treatment. The surfaces of the samples after the treatment became significantly smoother (see figure 9).

#### 4. Conclusions

An MNC (Ph-MNC) was synthesized based on an inexpensive PhCP in a facile process by the formation of iron oxide NPs in a polymer matrix from the soluble precursors. The presence of functional groups, porous structure, and the rough surface of the polymer allowed adsorption of iron ions from

the solution followed by the formation of P–O–Fe bonds. Subsequent treatment with sodium hydroxide led to the formation of magnetic NPs within the polymer matrix. FTIR data proved that the composite containing iron-containing compounds was formed while XRD data indicated the presence of particles in the form of magnetite, maghemite, goethite, hematite, and ferrihydrite. AFM studies enabled the determination of the sizes of the NPs to be in the range of ca. 100–160 nm that also showed strong magnetic properties as mapped using MFM.

Thermal degradation of the nanocomposite was studied using TGA. The obtained TG curves clearly showed the presence of three degradation stages for both the PhCP and Ph-MNCT. The first stage of weight loss covers a wider temperature range and the values of weight loss were more than three times larger for the Ph-MNC as compared to the PhCP likely due to the presence of hydroxyl groups on the surface of the magnetic particles that linked more water molecules. However, the weight loss in the second stage was for the Ph-MNC roughly two times smaller than for the PhCP as magnetic NPs can interact stronger with the products of degradation at this stage (e.g. water, HCl). At higher temperatures (above 270 °C) the third weight loss stage characterized by almost the same weight loss for both samples was observed. It indicates that magnetic NPs do not react with the degradation products at this stage or the interactions lead to products that at such temperatures subsequently decompose. Kinetic parameters, such as  $E_a$  and  $A$  values, were

calculated according to the Friedman and OFW methods. The comparison of the plots of  $E_a$  versus fractional mass loss for the second and third stages of the PhCP and the Ph-MNC indicate that the magnetic NPs strongly influence the complex degradation mechanism of the nanocomposite.

The native and calcinated nanocomposites (C-Ph-MNC) were shown to exhibit strong magnetic properties due to the presence of uniformly distributed NPs as evidenced using AFM and MFM. Thus, thermal degradation of the studied nanocomposite may be considered as a method for obtaining phosphorus-containing magnetic materials that may be of high application potential as magnetically separable sorbents. The presented results indicate that thermal treatment may be also used for regeneration of used MNCs.

## Acknowledgments

The authors would like to thank the Science Development Foundation under the President of the Republic of Azerbaijan and the German Research Center for Environmental Health, Helmholtz Zentrum München, the Joint Mass Spectrometry Centre, and the Cooperation Group 'Comprehensive Molecular Analytics' for financial support. Part of the research was done when R Alosmanov joined the group of Prof S Zapotoczny under the Erasmus Mundus Electra program (financed by the European Union). The authors would like to thank G Abbaszade and K Wolski for their help in the measurements.

## ORCID iDs

S Zapotoczny  <https://orcid.org/0000-0001-6662-7621>

## References

- [1] Stark W J, Stoessel P R, Wohlleben W and Hafner A 2015 Industrial applications of nanoparticles *Chem. Soc. Rev.* **44** 5793–805
- [2] Joo S H and Zhao D Y 2017 Environmental dynamics of metal oxide nanoparticle in heterogeneous systems: a review *J. Hazard. Mater.* **322** 29–47
- [3] Song Y H, Li Y H, Xu Q and Liu Z 2017 Mesoporous silica nanoparticles for stimuli-responsive controlled drug delivery: advances, challenges, and outlook *Inter. J. Nanomed.* **12** 87–110
- [4] Kinge S, Crego-Calama M and Reinhoudt D N 2008 Self-assembling nanoparticles at surfaces and interfaces *ChemPhysChem* **9** 20–42
- [5] Schmid G 2004 *Nanoparticles: From Theory to Application* (New York: Wiley)
- [6] Wang Y, Guo J, Li L, Ge Y, Li B and Zhang Y 2017 High-loading Fe<sub>2</sub>O<sub>3</sub>/SWNT composite films for lithium-ion battery applications *Nanotechnology* **28** 345703
- [7] Liu Y, Liu B and Nie Z 2015 Concurrent self-assembly of amphiphiles into nanoarchitectures with increasing complexity *Nano Today* **10** 278–300
- [8] Balazs A C, Emrick T and Russel T P 2006 Nanoparticle polymer composites: where two small worlds meet *Science* **314** 1107–10
- [9] Nicolais L and Carotenuto G 2005 *Metal-Polymer Nanocomposites* (New York: Wiley)
- [10] Ma J, Hu J M, Li Z and Nan C W 2011 Recent progress in multiferroic magnetoelectric composites: from bulk to thin films *Adv. Mater.* **23** 1062–87
- [11] Coemy J M D 1999 Whither magnetic materials? *J. Magn. Mater.* **196–197** 1–7
- [12] Novakova A A et al 2003 Magnetic properties of polymer nanocomposites containing iron oxide nanoparticles *J. Magn. Mater.* **258** 354–7
- [13] Szpak A, Kania G, Skórka T, Tokarz W, Zapotoczny S and Nowakowska M 2013 Stable aqueous dispersion of superparamagnetic iron oxide nanoparticles protected by charged chitosan derivatives *J. Nanopart. Res.* **15** 1372–83
- [14] Kania G et al 2018 Uptake and bioreactivity of charged chitosan-coated superparamagnetic nanoparticles as promising contrast agents for magnetic resonance imaging *Nanomedicine* **14** 131–40
- [15] Xu C, Zhang C, Wang Y, Li L, Li L and Whittaker A K 2017 Controllable synthesis of a novel magnetic core-shell nanoparticle for dual-modal imaging and pH-responsive drug delivery *Nanotechnology* **28** 495101
- [16] Kesavan M P et al 2017 Magnetic iron oxide nanoparticles (MIONs) cross-linked natural polymer-based hybrid gel beads: controlled nano anti-TB drug delivery application *J. Biomed. Mater. Res. Part A* (<https://doi.org/10.1002/jbm.a.36306>)
- [17] Hervault A and Thanh N T 2014 Magnetic nanoparticle-based therapeutic agents for thermochemotherapy treatment of cancer *Nanoscale* **6** 11553–73
- [18] Mornet S, Elissalde C, Bidault O, Weill F, Sellier E, Nguyen O and Maglione M 2007 Ferroelectric-based nanocomposites: toward multifunctional materials *Chem. Mater.* **19** 987–92
- [19] Alguero M et al 2014 Thin film multiferroic nanocomposites by ion implantation *ACS Appl. Mater. Interfaces* **6** 1909–15
- [20] Menini L, Pereira M C, Ferreira A C, Fabris J D and Gusevskaya E V 2011 Cobalt-iron magnetic composites as heterogeneous catalysts for the aerobic oxidation of thiols under alkali free conditions *Appl. Catal. A* **392** 151–7
- [21] Leung K C, Sham K W, Chak C P, Lai J M, Lee S F, Wang Y X and Cheng C H 2015 Evaluation of biocompatible alginate- and deferoxamine-coated ternary composites for magnetic resonance imaging and gene delivery into glioblastoma cells *Quant. Imaging Med. Surg.* **5** 382–91
- [22] Cho D-W, Jeon B-H, Chon C-M, Schwartz F W, Jeong Y and Song H 2015 Magnetic chitosan composite for adsorption of cationic and anionic dyes in aqueous solution *J. Ind. Eng. Chem.* **28** 60–6
- [23] Kalia S, Kango S, Kumar A, Haldorai Y, Kumari B and Kumar R 2014 Magnetic polymer nanocomposites for environmental and biomedical applications *Colloid Polym. Sci.* **292** 2025–52
- [24] Zapotoczny S, Szczubińska K and Nowakowska M 2015 Nanoparticles in endothelial theranostics *Pharmacol. Rep.* **67** 751–5
- [25] Gubin S P, Koksharov Y A, Khomutov G B and Yurkov G Y 2005 Magnetic nanoparticles: preparation, structure and properties *Russ. Chem. Rev.* **74** 489–520
- [26] Behrens S and Appel I 2016 Magnetic nanocomposites *Curr. Opin. Biotechnol.* **39** 89–96
- [27] Sun Z, Zhou X, Luo W, Yue Q, Zhang Y, Cheng X, Li W, Kong B, Deng Y and Zhao D 2016 Interfacial engineering of magnetic particles with porous shells: towards magnetic core-porous shell microparticles *Nanotoday* **11** 464–82
- [28] Liu C, Qu C, Wang D, Feng H, Liu P and Zhang Y 2015 Preparation and characterization of magnetic polyimide composite films copolymerized with aminophthalocyanine-coated Fe<sub>3</sub>O<sub>4</sub> nanocrystals *J. Mater. Sci., Mater. Electron.* **26** 4005–14

- [29] Dong S, Xu M, Wei J, Yang X and Liu X 2014 The preparation and wide frequency microwave absorbing properties of tri-substituted-bisphthalonitrile/Fe<sub>3</sub>O<sub>4</sub> magnetic hybrid microspheres *J. Magn. Mater.* **349** 15–20
- [30] Ziolo R F, Giannelis E P, Weinstein B A, Ohoro M P, Ganguly B N, Mehrotra V, Russell M W and Huffman D R 1992 Matrix-mediated synthesis of nanocrystalline gamma-Fe<sub>2</sub>O<sub>3</sub>—a new optically transparent magnetic material *Science* **257** 219–23
- [31] Sarkar S, Blaney L B, Gupta A, Ghosh D and SenGupta A K 2007 Use of ArsenXnp, a hybrid anion exchanger, for arsenic removal in remote villages in the Indian subcontinent *React. Funct. Polym.* **67** 1599–611
- [32] Rodriguez A F R, Coaquira J A H, Santos J G, Silveira L B, Marmolejo E M, Trennenpohl W, Rabelo D, Oliveira A C, Garg V K and Morais P C 2009 Characterization of magnetite nanoparticles supported in sulfonated styrene-divinylbenzene mesoporous copolymer *Hyperfine Interact.* **191** 417–23
- [33] Jacukowicz-Sobala I, Wilk Ł J, Drabent K and Kociolek-Balawejder E 2015 Synthesis and characterization of hybrid materials containing iron oxide for removal of sulfides from water *J. Colloid Interface Sci.* **460** 154–63
- [34] Suber L, Foglia S, Ingo G M and Boukos N 2001 Synthesis, and structural and morphological characterization of iron oxide-ion-exchange resin and -cellulose nanocomposites *Appl. Organometal. Chem.* **15** 414–20
- [35] Jacukowicz-Sobala I, Drabent K and Kociolek-Balawejder E 2015 Evaluation of ferromagnetic hybrid polymers obtained using cation exchangers *Mater. Chem. Phys.* **161** 107–15
- [36] Jacukowicz-Sobala I, Ciechanowska A and Kociolek-Balawejder E 2014 Hybrid polymer containing ferric oxides obtained using a redox polymer: I. Synthesis and characterization *Polimery* **59** 131–5
- [37] Alosmanov R M and Azizov A A 2012 Sorption isotherms of Nickel(II), Cobalt(II), Mercury(II), and Lead(II) ions on a phosphorus-containing polymeric sorbent *Russ. J. Inorg. Chem.* **57** 303–5
- [38] Yilmaz E, Alosmanov R M and Soylak M 2015 Magnetic solid phase extraction of lead(II) and cadmium(II) on a magnetic phosphorus-containing polymer (M-PhCP) for their microsampling flame atomic absorption spectrometric determinations *RSC Adv.* **5** 33801–8
- [39] Alosmanov R M, Azizov A A and Magerramov A M 2011 NMR spectroscopic study of phosphorus-containing polymer sorbent *Russ. J. Gen. Chem.* **81** 1477–9
- [40] Ahn T, Kim J H, Yang H-M, Lee J W and Kim J-D 2012 Formation pathways of magnetite nanoparticles by coprecipitation method *J. Phys. Chem. C* **116** 6069–76
- [41] Karami H 2010 Synthesis and characterization of iron oxide nanoparticles by solid state chemical reaction method *J. Clust. Sci.* **21** 11–20
- [42] Wu W, Wu Z, Yu T, Jiang C and Kim W 2015 Recent progress on magnetic iron oxide nanoparticles: synthesis, surface functional strategies and biomedical applications *Sci. Technol. Adv. Mater.* **16** 1–43
- [43] Tang J, Myers M, Bosnick K A and Brus L E 2003 Magnetite Fe<sub>3</sub>O<sub>4</sub> nanocrystals: spectroscopic observation of aqueous oxidation kinetics *J. Phys. Chem. B* **107** 7501–6
- [44] Schwertmann U and Cornell R M 2000 *Iron Oxides in the Laboratory* 2nd edn (Weinheim: Wiley)
- [45] Hua M, Zhang S, Pan B, Zhang W, Lv L and Zhang Q 2012 Heavy metal removal from water/wastewater by nanosized metal oxides: a review *J. Hazard. Mater.* **211–212** 317–31
- [46] Ercuta A and Chirita M 2013 Highly crystalline porous magnetite and vacancy-ordered maghemite microcrystals of rhombohedral habit *J. Cryst. Growth* **380** 182–6
- [47] Ma M, Zhang Y, Yu W, Shen H, Zhang H and Gu N 2003 Preparation and characterization of magnetite nanoparticles coated by amino silane *Colloid Surf. A* **212** 219–26
- [48] Zayed M A, Ahmed M A, Imam N G and El Sherbiny D H 2016 Preparation and structure characterization of hematite/magnetite ferro-fluid nanocomposites for hyperthermia purposes *J. Mol. Liq.* **222** 895–905
- [49] Hwang S W, Umar A, Dar G N, Kim S H and Badran R I 2014 Synthesis and characterization of iron oxide nanoparticle for phenyl hydrazine sensor applications *Sensor Lett.* **12** 1–5
- [50] Suzuki T, Hashimoto H, Itadani A, Matsumoto N, Kunoh H and Takada J 2012 Silicon and phosphorus linkage with iron via oxygen in the amorphous matrix of *Gallionella ferruginea* stalks *Appl. Environ. Microbiol.* **78** 236–41
- [51] Li Y S, Church J S and Woodhead A L 2012 Infrared and Raman spectroscopic studies on iron oxide magnetic nanoparticles and their surface modifications *J. Magn. Mater.* **324** 1543–50
- [52] Ozawa T A 1965 A new method of analyzing thermogravimetric data *Bull. Chem. Soc. Jpn.* **38** 1881–6
- [53] Flynn J H and Wall L A 1966 A quick direct method for the determination of activation energy from thermogravimetric data *J. Polym. Sci. C Polym. Lett.* **4** 323–8
- [54] Popescu C 1996 Integral method to analyse the kinetics of heterogeneous reactions under non-isothermal conditions. A variant on the Ozawa–Flynn–Wall method *Thermochim. Acta* **285** 309–23
- [55] Friedman H L 1964 Kinetics of thermal degradation of char-forming plastics from thermogravimetry: application to a phenolic plastics *J. Polym. Sci.* **6** 183–95
- [56] Arkhangel'skii I V, Dunaev A V, Makarenko I V, Tikhonov N A, Belyaev S S and Tarasov A V 2013 *Non-Isothermal Kinetic Methods Workbook and Laboratory Manual* (Edition Open Access: Berlin)
- [57] Silverstein R M, Webster F X, Kiemle D J and Bryce D L 2014 *Spectrometric Identification of Organic Compounds* 8th edn (Hoboken, NJ: Wiley)
- [58] Tudorachi N and Bunia I 2015 Synthesis and thermal investigation by TG–FTIR–MS analysis of some functionalized acrylic copolymers and magnetic composites with Fe<sub>3</sub>O<sub>4</sub> *J. Anal. Appl. Pyrolysis* **116** 190–201